

A theoretical and experimental kinetic study of phenyl radical addition to butadiene

Huzeifa Ismail^a, J. Park^b, Bryan M. Wong^a,
William H. Green Jr.^{a,*}, M.C. Lin^b

^a Department of Chemical Engineering, Massachusetts Institute of Technology, 25 Ames Street,
Cambridge, MA 02139, USA

^b Department of Chemistry, Emory University, 1515 Dickey Drive, Atlanta, GA 30320, USA

Abstract

The reactions of phenyl radical (C_6H_5) are of growing technological and scientific interest. A better understanding of phenyl radical addition to unsaturated hydrocarbons is of great practical interest because it is believed to be an essential component in both soot and fullerene formation. In this study, the rate of phenyl radical addition to butadiene was measured, and the potential surface of the reaction $C_6H_5 + C_4H_6$ was explored using quantum chemistry with the B3LYP density functional. Vibrational analysis allowed the determination of thermodynamic data and deduction of high-pressure-limit rate constants via transition-state theory. The pressure and temperature dependences of this chemically activated reaction were computed using a weak collision master equation analysis. The comparison of the predictions for the $C_6H_5 + C_4H_6$ system with experimental data showed good agreement. The rate constant for disappearance of phenyl radical was found to be $(3.16 \pm 0.29) \times 10^{12} \text{ cm}^3/\text{mol} \cdot \text{s} \exp[-(870 \pm 30)/T]$ over the temperature range 298–450 K. The dominant product at low temperature is the initial adduct, 4-phenylbuten-3-yl. Around 1000 K, the dominant product is phenyl butadiene formed from the chemically activated adduct, even at 10 atm. Above about 1400 K, bimolecular H-abstraction to form benzene is the most important process. Other products such as 1,4-dihydronaphthalene are much less important.

© 2004 The Combustion Institute. Published by Elsevier Inc. All rights reserved.

Keywords: Master equation; 1,4-Dihydronaphthalene; Phenyl; 1,3-Butadiene

1. Introduction

A fundamental understanding of soot and polycyclic aromatic hydrocarbon (PAH) formation is of great practical importance. For example, PAHs such as benzo[a]pyrene have been implicated in the development of lung cancer [1]. Furthermore, the formation of soot is an important component in the chemistry of combustion [2].

In particular, phenyl radical (C_6H_5) is believed to be a most important reactive precursor to soot formation in hydrocarbon combustion reactions. A quantitative understanding of the formation of larger PAH molecules, leading ultimately to soot particles, is essential for a better design of efficient and clean practical combustion devices such as engines or incinerators [3]. Extensive research over the last decades has addressed pathways leading to PAH of increasing size and ultimately soot has not included reaction of phenyl with 1,3-butadiene [4]. In particular, the simple

* Corresponding author. Fax: +1 617 324 0066.

E-mail address: whgreen@mit.edu (W.H. Green).

addition of phenyl radical to butadiene has not been reported to date in the literature.

Herein, we investigate the addition of phenyl radical to butadiene using an experimental and computational approach. The reaction of C_6H_5 with C_4H_6 can initially form several different products including $C_6H_6 + CH_2CHCHCH$, $C_6H_6 + CH_2CHCCH_2$, $C_6H_5CH_2CHCHCH_2$, and $C_6H_5CH(CH_2)CHCH_2$. The latter two adducts will be highly energized and might undergo several rapid unimolecular reactions, forming a wide variety of possible products before being collisionally quenched. Such unimolecular reactions may significantly contribute to the formation of naphthalene and in a similar manner to larger PAH, likely precursors of carbonaceous material such as soot [4]. However, neither the overall reaction rate between phenyl radical and butadiene nor the product branching ratios are known. In kinetic modeling of such large molecules, it is often assumed the reaction is in the high-pressure limit; that is, only the four channels listed above have significant yields. However, recent work has demonstrated that rather large molecules are indeed involved in chemically activated, pressure-dependent reactions, particularly at high temperatures [5]. In this work, the rate constants for important reactions in the $C_6H_5 + C_4H_6$ system are calculated as an explicit function of the temperatures and pressures of interest.

The predictions of a theoretical model should be consistent with that of the experimental observations to which the model is applied. Therefore, a comparison of computed kinetic models with experimental data is absolutely needed. Here, the cavity-ringdown spectroscopic (CRDS) method is used to directly measure the total loss rate of phenyl radical due to reaction with butadiene. This work concludes with a comparison of theoretical rate constants against experimental data.

2. Experimental methodology

The experiment was carried out using the cavity-ringdown spectrometric technique at the total pressure of 40 Torr. Detailed descriptions of the CRDS technique for kinetic applications have been reported in our earlier publications [6,7], and only a brief description will be given here.

All experiments were performed under slow-flow conditions using Ar as the carrier gas in a temperature-controlled reaction cell of about 570 cm^3 wrapped with resistive heaters. The reactor temperature, maintained within $\pm 0.7\text{ K}$, was measured with a calibrated K-type thermocouple (Alumel–Chromel) located below the center of the probe region. A Pyrex glass flow reactor with two pairs of laser windows attached opposite each other, permitting two-split photolysis laser beams to cross at the center of the reactor at a 30° angle,

was vacuum-sealed at the ends with a pair of highly reflective mirrors ($R = 0.9999$ at 500 nm, radius of curvature 6 m). This high-quality optical cavity approximately 50 cm in length can lengthen a pulse of probing dye laser operating at 500 nm with FWHM $\sim 10\text{ ns}$ to about $30\text{ }\mu\text{s}$.

Two pulsed lasers were employed, one for the generation of the C_6H_5 radical and the other for its detection. For radical generation from nitrosobenzene (C_6H_5NO) as the precursor, we employed a Lambda Physik KrF excimer laser (EMG 102) at 248 nm with an unfocused beam and 30–50 mJ in each $\sim 50\text{ ns}$ pulse. For probing the C_6H_5 radical, a Lambda Physik excimer laser (EMG 201) pumped tunable dye laser (FL 3002) was used. As reported by Porter and Ward [8], two strong absorption peaks were observed at 504.8 and 505.1 nm, and we utilized the stronger absorption at 504.8 nm ($^2B_1 \leftarrow ^2A_1$) for all of our kinetic studies. The 504.8 nm probe laser light was injected directly into the reactor cavity through one of the mirrors along the axis of the reactor tube. A fraction of the photon pulse transmitted through the second mirror was filtered and detected with a Hamamatsu photomultiplier tube (PMT). The photoelectric signal from the PMT was amplified with a fast preamplifier (SR445), and acquired and averaged with a multi-channel digital oscilloscope (LeCroy 140). The averaged signal was stored in a computer for future data analysis. A pulse-delay generator (SR DG 535) interfaced with the computer using LabView software was employed to control the firing of the two lasers as well as the triggering of the data acquisition system. To measure kinetics, the time delay between the two lasers was varied.

The concentration of each individual molecule was obtained by the following formula: $[R] = 9.66 \times 10^{16} (\%) PF_R/TF_T \text{ molecules/cm}^3$, where % is the percentage of each molecule in its gas mixture, P is the total reaction pressure in Torr, T is the reaction temperature, F_R is the flow rate of each gas mixture, and F_T is the total flowrate of all gases. The typical resident time in the probing zone was 10–40 ms, and the repetition rate of 2 Hz allowed enough time for a fresh sample in the reactor between pulses. The flowrates were measured by using mass flowmeters (MKS, 0258C), and the gas pressure was measured with an MKS Baratron manometer. The initial concentration of C_6H_5NO was determined by UV/VIS spectrometry (Shimadzu, UV-2401 PC) downstream of the reaction cell using standard calibration mixtures. Its concentrations ranged within $0.5\text{--}5.0 \times 10^{13} \text{ molecules/cm}^3$.

Butadiene (Aldrich, 99%) was purified by trap-to-trap distillation using appropriate slush baths before use. Nitrosobenzene (Aldrich, 97%) was purified by re-crystallization with ethanol at ice temperature, filtered, and dried in vacuum. Ar (Specialty Gases, 99.995% UHP grade) was used as the carrier gas without further purification.

3. Theoretical methodology

3.1. Quantum chemistry

The potential energy surface was explored, and computations on the reactants, reaction intermediates, products, and the corresponding transition states were performed using GAUSSIAN98 [9]. Calculations on reactant radicals and open shell transition states were done within the unrestricted formalism. Harmonic vibrational frequencies and optimized geometries were determined using the Becke [10] three-parameter hybrid functional combined with the Lee, Yang, and Parr [11] correlation (B3LYP) density functional theory method with the 6-31G(d,p) basis set. Although it is known in the literature that B3LYP underestimates barrier heights in general, the underestimation is not usually very large [12]. B3LYP has been repeatedly demonstrated to give rather accurate results for hydrocarbon structures, vibrational frequencies, and thermochemistry [13].

The standard rigid-rotor, harmonic-oscillator approximation was used to estimate the partition functions needed to compute the thermochemistry and rate constants, except many of the torsional modes were treated as large-amplitude rotors rather than small-amplitude harmonic vibrations. The low-frequency torsions about single bonds were treated as free internal rotors. Torsions with vibrational frequencies greater than 300 cm^{-1} were treated as harmonic oscillators (with statistical corrections for the number of low-energy conformations). A few of the higher-frequency torsional vibrations were treated as hindered internal rotors. The computed B3LYP harmonic vibrational frequencies were scaled by 0.9613 as recommended in the literature [14].

3.2. Rate constant calculations

The high-pressure-limit rate constants were calculated from conventional (fixed geometry) canonical transition-state theory:

$$k = \alpha \kappa(T) \left(\frac{k_B T}{h} \right) \frac{(Q^\ddagger/V)}{\prod_{i=1}^{N_{\text{reactants}}} (Q_i/V)} e^{-E_0/RT}, \quad (1)$$

where α is the reaction path degeneracy, $\kappa(T)$ is the Wigner tunneling correction factor corresponding to the magnitude of the imaginary frequency at the activated complex, T is the temperature, and E_0 is the zero-point-corrected barrier height. Q_i/V denotes the total partition function per unit volume of the i th reactant at the zero-point energy of the motionless reactant. Q^\ddagger/V is the corresponding partition function of the activated complex. The α was computed using symmetry numbers of the reactants and transition states such that it satisfied detailed balance as suggested by Pollak and Pechukas [15]. The moments of inertia for all internal rotors were calculated

using the $m = 2, n = 3$, Pitzer–Gwinn formulation [16,17]. The resulting high-pressure-limit rate constants $k_\infty(T)$ were fitted to the expression $k_\infty(T) = AT^n \exp(-E_a/RT)$ over a temperature range from 300 to 1800 K. The DFT energies added to the zero-point vibrational energy and the temperature-dependent enthalpy correction were used to determine reaction enthalpies of isodesmic reactions [18]; i.e., reactions that maintain the overall number and types of bonds. With a careful choice of isodesmic reactions, heats of formation can be evaluated to accuracies approaching uncertainties in experimental values. The thermodynamic properties of all species considered in the present work are summarized in Table 1 with available experimental values for phenyl and butadiene. Heats of formation were calculated through isodesmic reactions using methane, methyl, ethane, ethyl, ethylene, and vinyl as the reference compounds.

Microcanonical RRKM rate constants from statistical theory were calculated with the ChemRate v.1.9 program available from NIST [20]. Chemical activation, isomerization, and decomposition were accounted for in the program through the solution of the time-dependent master equation

$$\frac{d\rho_i^\alpha}{dt} = \omega \sum_j P_{ij}^\alpha \rho_j^\alpha - \omega \sum_j P_{ji}^\alpha \rho_i^\alpha - k_i^\alpha \rho_i^\alpha + \sum_\beta k_l^\beta \rho_l^\beta + R_l, \quad (2)$$

where ρ_i^α is the molecular population of isomer α at energy level E_i , ω is the collision frequency, P_{ij}^α is the collisional energy transfer probability from energy level j to energy level i of isomer α , k_i^α is the sum of rates for all the decomposition and isomerization channels from energy level E_i , k_l^β is the rate of isomerization from isomer β at energy E_l to isomer α at energy level E_i , and R_l is the chemical activation flux, which is assumed to be constant. Index l for isomer β corresponds to the same energy as i for α , i.e. $E_l = E_i$.


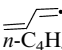
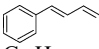
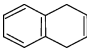
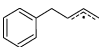
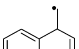
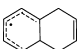
The first step in the main reaction sequence was the formation of the chemically activated molecule 4-phenyl-buten-3-yl from phenyl and butadiene. Both of the reactants were assumed to have a canonical distribution, i.e., a Boltzmann distribution. Energy transfer was modeled by weak molecular collisions with energy transfer probabilities given by the exponential-down model [21] with $\langle \Delta E \rangle_{\text{down}} = 400\text{ cm}^{-1}$. The Lennard-Jones parameters used were $[\sigma(\text{Ar}) = 3.54\text{ \AA}, \epsilon/k_B(\text{Ar}) = 93.3\text{ K}]$ [22] for Ar and $\sigma = 5.64\text{ \AA}, \epsilon/k_B = 450.0\text{ K}$ for all the isomers [23]. The master equation can be written in the matrix form

$$\frac{d\rho}{dt} = B\rho + R \quad (3)$$

and its solution is a function of the eigenvalues and eigenvectors of the relaxation matrix B [24]. The energy bin size used was $\delta E = 100\text{ cm}^{-1}$. The

Table 1

Ideal gas thermochemical parameters of selected molecules and radicals relevant to this study computed at the B3LYP 6-31G(d,p) level of theory

| Species | Formula | $\Delta_f H_0^0$ (kJ/mol) | S_{298}^0 (J mol ⁻¹ K ⁻¹) | $\Delta_f H_{298}^0$ (kJ/mol) | $\Delta_f H_{298}^0$ expt (kJ/mol) |
|----------------------------|--|------------------------------|---|----------------------------------|---------------------------------------|
| Hydrogen | H | 216.23 | 114.72 | 217.99 ^a | 217.99 [19] |
| 1,3-Butadien-2-yl |  <i>i</i> -C ₄ H ₄ | 308.90 | 292.14 | 299.07 | — |
| 1,3-Butadien-1-yl |  <i>n</i> -C ₄ H ₄ | 372.48 | 289.44 | 362.16 | — |
| 1,3-Butadiene | C ₄ H ₆ | 121.48 | 284.03 | 107.00 ^a | 108.78 [19] |
| Phenyl | C ₆ H ₅ | 336.89 | 289.98 | 323.76 ^a | 337.23 [19] |
| 1-Phenyl-1,3-butadiene |  C ₁₀ H ₁₀ | 211.76 | 413.34 | 185.39 | — |
| 1,4-Dihydro-naphthalene |  C ₁₀ H ₁₀ | 171.86 | 364.43 | 142.55 | — |
| 4-Phenyl-buten-3-yl |  C ₁₀ H ₁₁ | 270.42 | 438.25 | 239.45 | — |
| 3-Phenyl-buten-4-yl |  C ₁₀ H ₁₁ | 356.61 | 438.67 | 326.69 | — |
| 1,4,9-Trihydro-naphthalene |  C ₁₀ H ₁₁ | 316.03 | 376.52 | 283.30 | — |

^a Other values have been reported in the literature, but these values are used on the potential energy surface for consistency.

default for E_{\min} was 64.63 kcal, and E_{\max} was set at 370.00 kcal. The resulting matrix size of 2098 × 2098 was tested to ensure convergence.

As discussed by Knyazev and Tsang [25], the rate constants inferred from the solution of the master equation vary with time. However, time ranges exist where the computed rate constants are indeed constant, and if these timescales are used, the rate constants computed by solving the time-dependent equations are (at least in this case) very similar to the values obtained from steady-state solutions. In the present case, solutions of the time-dependent equations were examined in the microsecond-to-millisecond time range, where the rate constants were truly constant. At shorter timescales, the results are convolved with vibrational relaxation; at longer timescales, thermal dissociation of the stabilized adducts confuses the interpretation.

The decomposition reactions were treated as irreversible (“infinite sink” approximation). The isomerization reactions were defined as reversible. To correct for reversibility, the “subtract in-

comes” option in ChemRate v.1.9 was used to obtain effective (net) isomerization rate constants from the total isomerization fluxes in the forward and reverse directions. The use of the net isomerization rate constants simplifies the analysis of product branching, because any reversible isomerization can be treated as an “irreversible” process with an effective rate constant, which is already corrected for the reversibility. Then for a kinetic model of arbitrary complexity consisting of chemical activation followed by a sequence of effectively irreversible reactions, the apparent rate constants are calculated as the products of the total (chemical activation) rate constant and appropriate branching fractions at each well.¹

¹ With the “subtract incomes” option, the branching ratios need to be manually calculated in ChemRate version 1.9; the numbers reported in the user interface are confusing. This bug will be corrected in future versions of ChemRate.

4. Results and discussion

4.1. Experimental results

For kinetic measurements, the CRDS method provides the decay times of the injected probing photons in the absence (t_c^0) and the presence (t_c) of absorbing species. The typical photon decay curves are shown in the inset of Fig. 1. These photon decay times can be related to the concentration of the species at time t after its generation by the equation

$$1/t_c = 1/t_c^0 + B[A]_0 e^{-kt} \quad (4)$$

or

$$\ln(1/t_c - 1/t_c^0) = C - kt, \quad (5)$$

where $[A]_0$ is the initial concentration of the radical species of interest, C_6H_5 , B is a constant that contains experimental parameters such as the cavity length (50 cm), the refractive index of the absorbing medium, etc., and $C = \ln(B[A]_0)$. The initial concentration of phenyl was estimated to be in the range of $1\text{--}5 \times 10^{12}$ radicals/cm³. Eq. (5) is valid, provided the decay time of the species of interest is much longer than that of photons within the cavity. This condition can be readily met because the chemical decay time, typically in the range of several hundreds of microseconds to tens of milliseconds, can be controlled by the concentration of the molecular reagent.

The slopes of the $\ln(1/t_c - 1/t_c^0)$ vs t plots, as illustrated in Fig. 1 for the reactions of C_6H_5 with butadiene, yield the pseudo-first-order rate coefficients, k' , for the decay of C_6H_5 in the presence of known excess 1,3- C_4H_6 concentrations as specified. A standard plot of k' vs reagent concentration is shown in Fig. 2, which gives the averaged

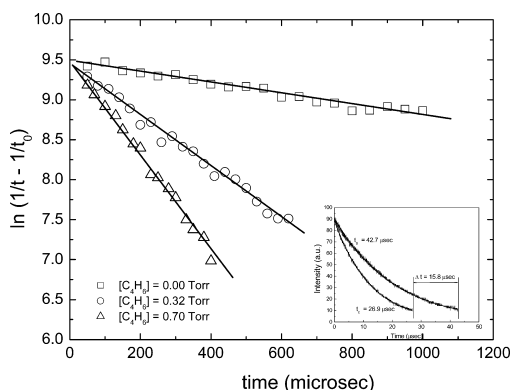


Fig. 1. Typical pseudo-first-order decay plots for the reaction of C_6H_5 with C_4H_6 at 301 K. The inset is a typical photon decay curves with (top) and without (below) absorbing species. The bold curves are exponentially fitted curves.

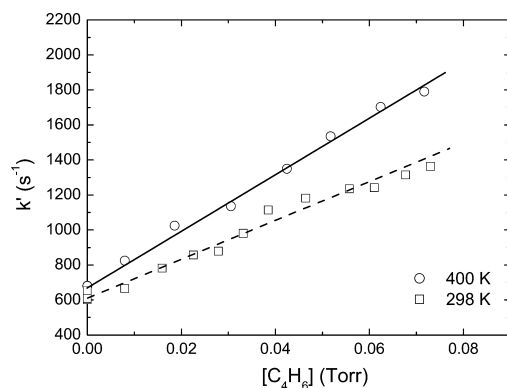


Fig. 2. Typical k' vs $[C_4H_6]$ plot.

second-order rate constant k'' from its slope according to the relationship

$$k' = k^0 + k''[X], \quad (6)$$

where k^0 is the radical decay constant in the absence of the molecular reactant X ; this is thought to be due to the loss of the radical by diffusion away from the probing beam and from recombination reactions (e.g., $C_6H_5 + NO$ and $C_6H_5 + C_6H_5$).

The bimolecular rate constants determined from the slopes of k' vs concentration plots are given in Fig. 3 and Table 2. Weighted least-squares analysis of the individual set of reaction rate constants gave rise to the following expression, in units of cm³/(mol s):

$$k = (3.16 \pm 0.29) \times 10^{12} \exp[-(870 \pm 30)/T]. \quad (7)$$

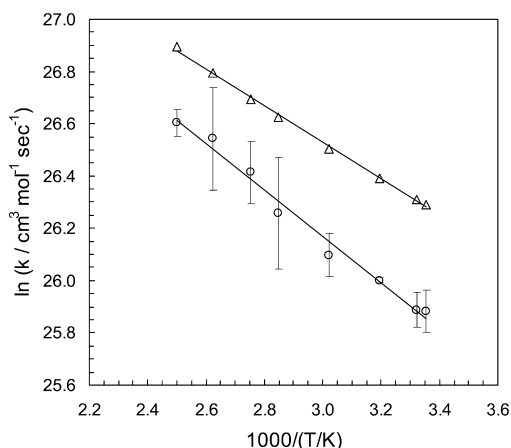


Fig. 3. Arrhenius plots of the overall rate constant for the $C_6H_5 + C_4H_6$ reaction, from theory (Δ) and experiment (\circ).

4.2. Theoretical results

The reaction pathways studied are shown in Fig. 4. This network is of course not complete; the large number of isomers and an even larger number of reactions interconnecting these isomers make a complete investigation of the potential energy surface impractical. Therefore, only the most probable reaction pathways were considered.

The addition of phenyl to the terminal carbons of butadiene, via **TS1**, is the most important reaction path. According to our quantum calculations, this path is barrierless, but there is a significant T -dependence of the rate due to the difference between the T -dependence of the partition function of the TS and the partition function of the reactants (primarily due to the T -dependence of the internal rotor partition functions). The theoretical T -dependence is slightly weaker than that observed experimentally, suggesting that either there is a small barrier ($\sim 2 \pm \sim 5$ kJ/mol). The error is due to accumulation of uncertainties in our calculations.

The internal rotation of butadiene was treated as a double minimum hindered rotor, where the barrier between the *trans* to *cis* isomerization was found to be 27.41 kJ/mol. Species 3^\ddagger is internally excited, and can potentially undergo several isomerization and decomposition reactions before being

stabilized. Species 3^\ddagger was treated as a double minimum hindered rotor with a high barrier of 64.31 kJ/mol because of the partial double bond. This is the input channel for the main chemically activated reaction network. The H-abstraction pathway producing benzene and **8**, via **TS5**, is not competitive until quite high temperatures since its barrier is ~ 8 kJ/mol higher than the near-zero barrier for the addition to the terminal carbons. Addition to the interior carbons on butadiene forming 10^\ddagger , via **TS7**, was considered but it is even less significant since its barrier is higher (17 kJ/mol). Similarly, H-abstraction from the terminal carbons to produce benzene and **9** has a much higher barrier (9 kJ/mol) than H-abstraction from the interior carbons; therefore, it is not significant except at extremely high temperatures.

The most important portions of the potential energy surface are shown schematically in Fig. 5. The reaction channel through **TS1** is very exothermic due to the thermodynamically favorable resonance-stabilized product. Therefore, in accordance with Hammond's postulate, the transition-state structure is similar to that of the separated reactants. The energized adduct 3^\ddagger can lose a hydrogen atom, via **TS3**, to form 1-phenyl-1,3-butadiene (**5**). Alternatively, the energized adduct can cyclize to form the bicyclic radical 1,4,9-trihydronaphthalene (**4**) via **TS2**. The bicyclic radical then rapidly loses hydrogen to form 1,4-dihydronaphthalene (**6**).

The computed thermodynamic properties of all the species considered in the present work are given in Table 1. The molecular geometries and vibrational frequencies are available from the authors upon request. The high-pressure-limit rate constants corresponding to the transition states listed in Fig. 4 are shown in Table 3. At pressures of 0.01 and 10 atm, the computed apparent rate

Table 2
Measured bimolecular rate constant of C_6H_5 reaction with butadiene (C_4H_6)

| T (K) | $[C_4H_6]$ (Torr) | $k/10^{11}$ ($cm^3/mol\ s$) ^a |
|---------|-------------------|--|
| 298 | 0–0.073 | 1.74 ± 0.14 |
| 301 | 0–0.700 | 1.75 ± 0.12 |
| 313 | 0–0.077 | 1.96 ± 0.22 |
| 331 | 0–0.070 | 2.16 ± 0.18 |
| 351 | 0–0.064 | 2.53 ± 0.54 |
| 363 | 0–0.054 | 2.96 ± 0.36 |
| 381 | 0–0.074 | 3.37 ± 0.66 |
| 400 | 0–0.072 | 3.58 ± 0.18 |

^a All experiments were performed at 40 Torr using Ar carrier gas. The uncertainties represent 1σ , evaluated with weighted least-squares analyses by convoluting the errors in k' for k'' .

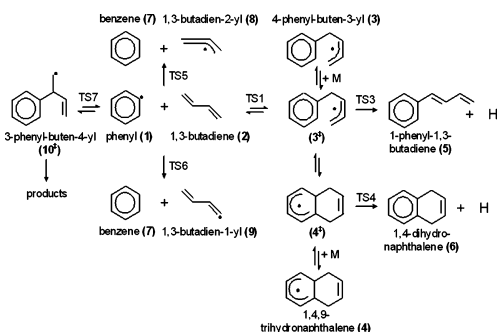


Fig. 4. Network of reaction pathways.

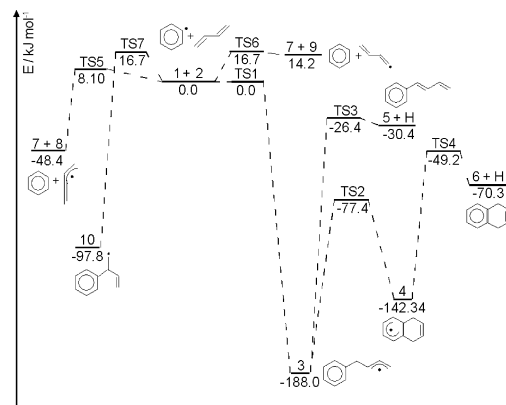


Fig. 5. Potential energy diagram for the chemically activated $C_6H_5 + C_4H_6$ reaction. ZPE-corrected energies (kJ/mol) at 0 K, relative to reaction **1 + 2**, are calculated by B3LYP 6-31G(d,p) basis.

Table 3

Transition-state theory rate constants^a for elementary reactions included in Fig. 4

| Reaction | Log ₁₀ (<i>A</i>) | <i>n</i> | <i>E_a</i> (kJ/mol) |
|---------------|--------------------------------|----------|-------------------------------|
| 1 + 2 → 3 | 5.91 | 2.56 | 0 ^b |
| 1 + 2 → 10 | 4.68 | 2.65 | 16.70 |
| 1 + 2 → 7 + 8 | 3.94 | 3.12 | 8.10 |
| 1 + 2 → 7 + 9 | 4.50 | 3.11 | 16.70 |
| 3 → 4 | 5.51 | 1.64 | 110.61 |
| 3 → 5 + H | 7.82 | 2.11 | 161.62 |
| 4 → 6 + H | 10.14 | 1.25 | 92.60 |

^a Fitted to the modified Arrhenius form $k = AT^n \exp(-E_a/RT)$. *A* is in mol, cm³, s units.^b The slope in Fig. 3 is primarily due to the *T*^{*n*} dependence of the partition functions. Combining the experimental *T*-dependence with the theoretical partition functions suggests $E_a \sim 2 \pm 5$ kJ/mol.

constants for the formation of the stabilized adduct (3) and of several isomers are shown in Figs. 6A and B. The experimental and computed *A*-factors are in excellent agreement where the former equals 3.31×10^{12} cm³/mol s and the latter equals 2.72×10^{12} cm³/mol s. The computed overall rate for loss of phenyl at 0.052 atm is compared with experiment in Fig. 3. The computed overall reaction rate is higher than the experimental data by about 50% at room temperature, with a slightly smaller deviation at higher temperatures. This is an excellent agreement considering computational uncertainties for this barrierless reaction, which was modeled rather simply using conventional (rather than variational) transition-state theory. The deviation may stem primarily from the underestimation of the addition barrier; an increase of 0.5 kcal/mol, for example, would result in a quantitative agreement between experiment and theory.

The master equation analysis shows the initial adduct (3) is the dominant product at low temperatures, and this reaction is in its high-pressure limit even at the low-pressure experimental conditions of 0.052 atm. According to the calculations, the rate of this reaction begins to fall off significantly above *T* = 580 K at 0.052 atm, and even at 10 atm the reaction is far from the high-pressure limit above 1000 K. This is consistent with published analyses of other chemically activated reactions of molecules in this size range [3].

The calculations show that 1-phenyl-1,3-butadiene (5) becomes the dominant product when 3 begins to fall off, but that at higher temperatures (*T* > 1400 K) the channels with significant entrance barriers, particularly H-abstraction from the interior carbons, become even more important. The bicyclic species 1,4-dihydronaphthalene (6), an isomer of 1-phenyl-1,3-butadiene, is predicted to be most important in the temperature range around 1000 K, where 1-phenyl-1,3-butadiene is the dominant channel; however, the chemically activated reactions forming the bicyclic species are always more than an order of magnitude slower than the main channels. It seems likely there are other more important reaction

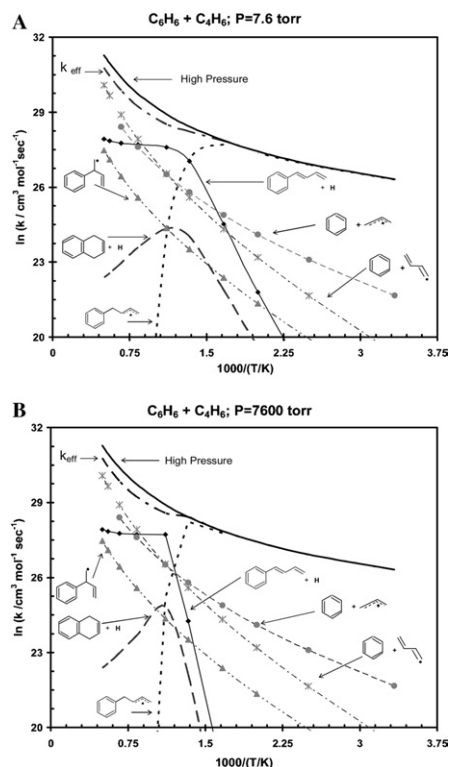


Fig. 6. Computed rates for the reaction $C_6H_5 + C_4H_6$ to form various products (A) $P = 7.6$ Torr, (B) $P = 7600$ Torr. The thermalized initial adduct 1 is the main product at low temperature, phenyl butadiene is the main product around 1000 K, and H-abstraction to form benzene becomes dominant at high temperatures. Ring closure is much slower than the main reaction channels. The k_{eff} is the effective rate constant for the formation of all the products from the initial adduct. The line labeled with 3-phenyl-buten-4-yl represents an upper bound on the sum of all the minor products, which can be formed through that adduct, see text.

paths to bicyclics even at 1000 K, possibly including subsequent bimolecular reactions of the major product thermalized 1-phenyl-1,3-butadiene.

5. Conclusions

The overall rate of phenyl addition to butadiene was measured directly with laser flash photolysis, using cavity-ringdown spectroscopy to probe the phenyl radical. In 40 Torr of Ar, over the temperature range 298–450 K, the rate constant is $k = (3.16 \pm 0.29)$

$$\times 10^{12} \text{ cm}^3/\text{mol s} \exp[-(870 \pm 30)/T]. \quad (8)$$

According to our calculations, this reaction is in the high-pressure limit under the experimental conditions, and the dominant product under these conditions is the adduct 4-phenyl-buten-3-yl.

The rate constant and product branching ratios for $\text{C}_6\text{H}_5 + \text{C}_4\text{H}_6$ under other conditions were predicted based on ab initio calculations. The potential energy surface was explored using B3LYP calculations. Transition states were determined, and rate constants were obtained by means of transition-state theory. Apparent rate constants for the various product channels were obtained from a master equation analysis at different pressures. The computed apparent rate constant for the disappearance of phenyl was within 50% of the experimental values. The master equation analysis showed the formation of the stabilized adduct is in its high-pressure limit for temperatures lower than 600 K even at $P = 0.01$ atm. Chemically activated product channels dominate around 1000 K, even at 10 atm, but simple H-abstraction to form benzene dominates above 1400 K. The bicyclic species 1,4,9-trihydronaphthalene and 1,4-dihydronaphthalene are minor products under all reaction conditions.

Acknowledgments

J.P. and M.C.L. acknowledge support by the Basic Energy Sciences, Department of Energy, under Grant No. DE-FG-97ER14784 to Emory University. H. Ismail, B.M. Wong, and W.H. Green acknowledge the support Office of Basic Energy Sciences, Office of Energy Research, U.S., DOE Grant No. DE-FG02-98ER14914 and NSF under Grant CTS-0123345. The authors are grateful to Joanna Yu for providing the isodesmic reactions employed in this study. We also gratefully acknowledge Dr. Igor Tokmakov for several helpful conversations.

References

- [1] M.F. Denissenko, A. Pao, M. Tang, G.P. Pfeifer, *Science* 274 (1996) 430–432.
- [2] M. Frenklach, *Phys. Chem. Chem. Phys.* 4 (2002) 2028–2037.
- [3] H. Richter, O.A. Mazzyar, R. Sumathi, W.H. Green, J.B. Howard, J.W. Bozzelli, *J. Phys. Chem. A* 105 (2001) 1561–1573.
- [4] H. Richter, J.B. Howard, *Prog. Energy Combust. Sci.* 26 (2000) 565–608.
- [5] B.M. Wong, D.M. Matheu, W.H. Green, *J. Phys. Chem. A* 107 (2003) 6206–6211.
- [6] T. Yu, M.C. Lin, *J. Am. Chem. Soc.* 116 (1994) 9571–9576.
- [7] J. Park, M.C. Lin, *ACS Symp. Ser.* 720 (1999) 196–209.
- [8] G. Porter, B. Ward, *Proc. R. Soc.* 457 (1965) 4287.
- [9] M.J. Frisch, G.W. Trucks, H.B. Schlegel, G.E. Scuseria, M.A. Robb, J.R. Cheeseman, V.G. Zakrzewski, J.A. Montgomery Jr., R.E. Stratmann, J.C. Burant, S. Dapprich, J.M. Millam, A.D. Daniels, K.N. Kudin, M.C. Strain, O. Farkas, J. Tomasi, V. Barone, M. Cossi, R. Cammi, B. Mennucci, C. Pomelli, C. Adamo, S. Clifford, J. Ochterski, G.A. Petersson, P.Y. Ayala, Q. Cui, K. Morokuma, D.K. Malick, A.D. Rabuck, K. Raghavachari, J.B. Foresman, J. Cioslowski, J.V. Ortiz, A.G. Baboul, B.B. Stefanov, G. Liu, A. Liashenko, P. Piskorz, I. Komaromi, R. Gomperts, R.L. Martin, D.J. Fox, T.A. Keith, M.A. Al-Laham, C.Y. Peng, A. Nanayakkara, C. Gonzalez, M. Challacombe, P.M.W. Gill, B.G. Johnson, W. Chen, M.W. Wong, J.L. Andres, M. Head-Gordon, E.S. Replogle, J.A. Pople, *Gaussian 98*, Rev. A.7, Gaussian, Inc., Pittsburgh, PA, 1998.
- [10] A.M. Becke, *J. Chem. Phys.* 98 (1993) 5648–5652.
- [11] C. Lee, W. Yang, R.G. Parr, *Phys. Rev. B* 37 (1988) 785–789.
- [12] C.D. Wijaya, R. Sumathi, W.H. Green Jr., *J. Phys. Chem. A* 107 (2003) 4908–4920.
- [13] G.A. Petersson, D.K. Malick, W.G. Wilson, J.W. Ochterski, J.A. Montgomery, M.J. Frisch, *J. Chem. Phys.* 109 (1998) 10570–10579.
- [14] A.P. Scott, L. Radom, *J. Phys. Chem.* 100 (1996) 16502–16513.
- [15] E. Pollak, P. Pechukas, *J. Am. Chem. Soc.* 100 (1978) 2984–2991.
- [16] K.S. Pitzer, W.D. Gwinn, *J. Chem. Phys.* 10 (1942) 428–440.
- [17] W.J. Hehre, R. Ditchfield, L. Randon, J.A. Pople, *J. Am. Chem. Soc.* 92 (16) (1970) 4796–4801.
- [18] A.L.L. East, L. Radom, *J. Chem. Phys.* 106 (1997) 6655–6673.
- [19] P.J. Linstrom, W.G. Mallard (Eds.), *NIST Chemistry WebBook*, NIST Standard Reference Database Number 69, National Institute of Standards and Technology, Gaithersburg, MD, July 2001. Available from: <<http://webbook.nist.gov>>.
- [20] V. Mokrushin, V. Bedanov, W. Tsang, M. Zachariah, V. Knyazev, *ChemRate Version 1.19*, National Institute of Standards and Technology, Gaithersburg, MD, 2002.
- [21] K.A. Holbrook, M.J. Pilling, S.H. Robertson, *Unimolecular Reactions*, second ed. Wiley, New York, 1996, p. 179.
- [22] R.C. Reid, J.M. Prausnitz, B.E. Poling, *The Properties of Gases and Liquids*, fourth ed. McGraw-Hill, New York, 1987, p. 733.
- [23] I.V. Tokmakov, M.C. Lin, *J. Am. Chem. Soc.* 125 (37) (2003) 11397–11408.
- [24] R.G. Gilbert, S.C. Smith, *Theory of Unimolecular and Recombination Reactions*. Blackwell, Oxford, 1990.
- [25] V.D. Knyazev, W. Tsang, *J. Phys. Chem. A* 103 (1999) 3944–3954.